JOURNAL OF MATERIALS SCIENCE 36 (2001) 4411–4418

The effect of the skin thickness and spherulite size on the mechanical properties of injection mouldings

J. C. VIANA, A. M. CUNHA
Polymer Engineering Department, University of Minho, 4800 Guimarães, Portugal
E-mail: jcv@dep.uminho.pt

N. BILLON
Centre de Mise en Forme des Matériaux, UMR CNRS 7635, École des Mines de Paris, BP207 06904, Sophia-Antipolis, France

In this work are studied the relationships between the microstructure and the mechanical properties of an injection moulded propylene-ethylene copolymer. Distinct microstructures were obtained by processing, through a moulding programme that includes the variation of the injection and the mould temperatures and the injection flow rate. They were characterized by the skin ratio (measured by polarised light microscopy) and the spherulite size (evaluated by small angle light scattering system). Tensile tests were carried out at two different constant loading velocities: 2 mm/min (3.33×10^{-5} m/s) and 3 m/s, in order to assess the initial modulus, the yield stress, the strain and the energy at break. The results are presented in terms of the relationships between the chosen microstructural parameters and the selected tensile properties. The skin thickness is evidenced as an important microstructural feature. The role of the core spherulite size is secondary or even negligible. The results also show that other microstructural parameters must be considered to establish more general microstructure-properties relationships.

1. Introduction

The mechanical properties of an injection moulded polymer are dependent on the microstructure developed upon the constrains imposed by the thermomechanical conditions during processing. An injection moulded semicrystalline polymer exhibits a typical layered-up microstructure through the thickness of the moulding, which is easily observable by polarised light microscopy [1, 2]. The number of identified layers is dependent on the level of discrimination considered and on the degree of resolution of the experimental technique used. The simplest analysis can reduce the number of layers to three [3, 4]: two highly oriented outer skin layers and a central spherulitic core; known as the skin-core laminate concept. The individual properties of each layer and their relative dimensions are controlled by the thermal and mechanical fields generated during the processing stages of filling, holding and cooling.

The influence of the microstructure on the mechanical properties can be assessed by various microstructural parameters. Several studies evidenced that the mechanical properties of injection mouldings can often be correlated to the skin thickness [3–5]. Obviously, this remains true as far as the skin morphology is significant different from the core material. In parallel, the effect of the spherulite size on the mechanical behaviour can efficiently be analysed using compressed mouldings [6, 7]. As far as some correlations can be found between these microstructural parameters and the mechanical properties [6, 8–10], the two above features can be looked as geometrical features that are associated to the macromolecular orientation of the skin and to the semicrystalline texture of the core, respectively.

The mechanical properties of moulded polymers also depend on the mode the solicitation [11, 12] and on the imposed strain rate [13, 14], being an open problem the understanding of the effect of the microstructure in those processes. However, it is well establish that in a tensile solicitation at constant loading velocity, both the properties of the skin and of the core layers will control the whole part response [11, 14], and that the influence of the microstructure on the mechanical properties is enhanced at high strain-rates [5, 13].

This work presents the relationships between the microstructure and the mechanical properties of an injection moulded propylene-ethylene copolymer. Specifically, it is studied the correlation between the skin thickness and the core spherulite size and the mechanical properties of the mouldings, evaluated by tensile tests at two different velocities. The variations of the

microstructure parameters were achieved by systematic variations of the processing conditions, namely, the melt and mould temperatures and the injection flow rate.

2. Microstructure development under processing

The complex thermomechanical environment imposed to the melt in injection moulding results mainly from the combined effect of: the high shear stress associated to the flow rate, to the moulding geometry and the material rheological properties; the high cooling rates resulting from the relatively low temperatures of the mould walls; and the pressure level of the holding stage. This environment constrains locally the microstructure development and, consequently, the individual properties of each layer of the skin-core structure.

2.1. Skin layer

The skin layers start to be formed during the filling stage due to the rapid cooling of the hot and oriented melt against to the cold mould walls. For PP and other polyolefins, the skin features a typical lamellar shish-kebab structure [3, 15–17], characteristic of the fast crystallization (driven by high cooling rates) of highly sheared flows. For a given flow rate prior crystallization, the skin formation is essentially governed by the balance between the local cooling time (as soon as crystallisation temperature is reached) and the relaxation time of the material [17]. The final level of molecular orientation of this layer results from both the orientation induced by flow (related to the imposed stress field) and the relaxation occurring thereafter [17, 18]. For injection moulded tensile bars, a direct correlation between the skin thickness and its level of orientation has been found [8, 9], with thicker skins including more oriented material. Consequently, the mechanical properties of the skin are the result of this high orientation level and of the type of crystalline structures developed under this constraint. As the skin exhibits a stiffer behaviour and a lower ductility than the core [3], the relative importance of this performance on the global properties of the specimen is then enhanced by the thickness of the skin.

The microstructural evolution from the skin to the core is progressive, and a transition zone can be defined in between. The morphology of this region is more dependent on the holding stage setup of the moulding cycle. During this stage, a flow still occurs to compensate for the material shrinkage associated to the density increment during cooling, and the polymer in the cavity is kept under pressure until the gate freezes. So, the material orientation patterns can be significantly altered due to the flow occurred at relatively low temperatures [9, 19], and to the constraints for melt relaxation. In general, a high density of β-type spherulites is found in this transition zone [3, 20], with a significant effect on the mechanical properties, especially at higher strain rates [11, 21, 22].

2.2. Core layer

The core layer of PP injection mouldings shows essentially an α-type spherulitic crystallization, typical of melts that crystallise in almost quiescent conditions. The previously formed skins act as an insulation barrier due the low thermal conductivity of the polymer, leading to a lower cooling rate of the core, and to a consequent higher degree of crystallinity [3]. A gradient of spherulite sizes is also formed, which increases towards the central zone. The dimensions of the spherulites are governed by the nucleation process [23]. It has been suggested that apparently the spherulite size effect is just a reflection of the crystallisation inside it (crystallinity, lamellar thickness, amorphous layer) and not of the state of the boundaries [10]. The core layer shows a low orientation level, being possible to consider it as almost isotropic. So, it normally shows a lower stiffness and higher deformation at break than the skin layer [3].

3. Experimental procedure

3.1. Material and moulding program

The material used in this work is a commercial grade of propylene-ethylene copolymer (APPRYL 3120 MR5). This is a sequential copolymer with narrow molecular weight distribution, and with a melt flow index of 11 g/600 s (230°C/21.6 N).

Specific axisymmetric dumbbell-like specimens [13, 17] were injection moulded, with systematic variations of three processing variables, namely: the melt temperature, T_{inj}, the mould temperature, T_m, and the flow rate, Q_{inj}. These were varied in 3 levels accordingly to a design of experiments plan (Face Central Composite). The Table I shows the selected level of the processing variables.

Details of the moulding programme can be found elsewhere [13]. A reference system was used to identify each of the different processing batches (e.g., 230/30/10 refers to the samples moulded with $T_{inj} = 230°C$, $T_m = 30°C$, and $Q_{inj} = 10\ cm^3/s$, respectively).

3.2. Microstructure characterization

From each moulded specimens, cross-sectional samples of 15 μm were microtomed transversely to the flow direction, using a LEITZ microtome with razor blades. These slices were observed in a polarised light microscope, coupled with a computer image analyser system QUANTIMED 500C. The skin thickness was determined as the average value of measurements in 10 different points. The skin ratio, S_a, was defined as

TABLE I Levels of variation of the processing variables

	Minimum	Medium	Maximum
T_{inj} (°C)	200	230	270
T_m (°C)	5	30	80
Q_{inj} (cm^3/s)	5	10	40

T_{inj}—melt temperature, T_m—mould temperature, Q_{inj}—injection flow rate.

the quotient between the cross sectional areas of the skin and of the total specimen:

$$S_a = \frac{2R_t t - t^2}{R_t^2} \quad (1)$$

where, R_t is the sample radius and t is the skin thickness.

The same microtomed sections used in the optical microscopy were also used in the SALS experiments. The average size of the spherulites in the core, R_s, was assessed by a small angle light scattering system (SALS), equipped with a HeNe laser beam (diameter of 0.8 mm and 632.8 nm of wave-length), from the obtained H_v scattered pattern (analyser and polariser crossed at 90°). The intensity variations along each lobe of the typical pattern obtained were measured in the image analyser after digitalisation of the acquired photographed pattern (the intensity was assumed to be proportional to the assessed grey level). R_s was estimated by [24]:

$$R_s = \frac{1.0025}{\pi} \frac{\lambda}{\sin(\theta/2)} \quad (2)$$

where λ is the light wavelength and θ the radial scattering angle ($\theta = \arctan(\frac{l}{d})$ with l the distance from the centre of the H_v pattern to the maximum of intensity in each lobe and d the sample-to-film distance).

3.3. Mechanical tests

The tensile tests were performed at two different test velocities. The low velocity tests (chosen to avoid self-heating of the sample during drawing) were carried out in an INSTRON 4505 universal testing machine at constant crosshead speed of 3.33×10^{-5} m/s (or 2 mm/min, given a nominal initial strain rate of 1.67×10^{-3} s^{-1}). At least 5 samples were tested for each moulding condition. The tensile-impact tests were performed in ZWICK-rel 1842 hydraulic machine, at a constant crosshead speed of 3 m/s (nominal initial strain rate of 1.50×10^{2} s^{-1}). At least 8 samples per condition were tested. Both tests were carried out at controlled room temperature (23°C). In all the cases, the obtained force-displacement, F-Δl, curves were converted in the homogeneous stress-strain curves, $\sigma_h - \varepsilon_h$. The mechanical parameters considered were the initial modulus, E, the yield stress, σ_y, the strain at break, ε_b, and the total energy at break per initial cross-sectional area of the specimen, u_b.

4. Results

4.1. Microstructure characterization

All the samples show the typical clear and well-defined skin-core structure when observed by polarised light microscopy. As expected, the thickness of the skin layer depends on the processing conditions [13, 17] (Fig. 1). The core microstructure is not discernible, even at higher magnifications, due to the very small size of the formed structures.

The associated SALS scattered patterns (Fig. 2) and grey level variations along the four lobes (each line corresponds to the two lobes resting in the same diameter) exhibit a significant deviation from the theoretical ones. This can be attributed to the heterogeneous microstructure developed upon processing (e.g., the distribution of spherulite sizes, the impingement and incomplete growth of spherulites and their internal disorder [24]) and to the multi-scattering phenomena (due to the relatively high thickness of the samples compared to the size of the scattering objects). The so-called degenerated patterns, obtained from samples containing very small and imperfect spherulites, have a non-zero central intensity and a circular link between the lobes that become wider as the spherulite becomes more truncated [24]. This leads to the experimental difficulty in localise the maximum intensity. However, the grey levels-radial distance plots (Fig. 2) show a change in the slope which is assumed to correspond to the maximum intensity locus, and its position was used in Equation 2 to comparatively estimate the values of R_s. Nevertheless, the spherulite dimensions are inversely proportional to the size of the scattered pattern. Furthermore,

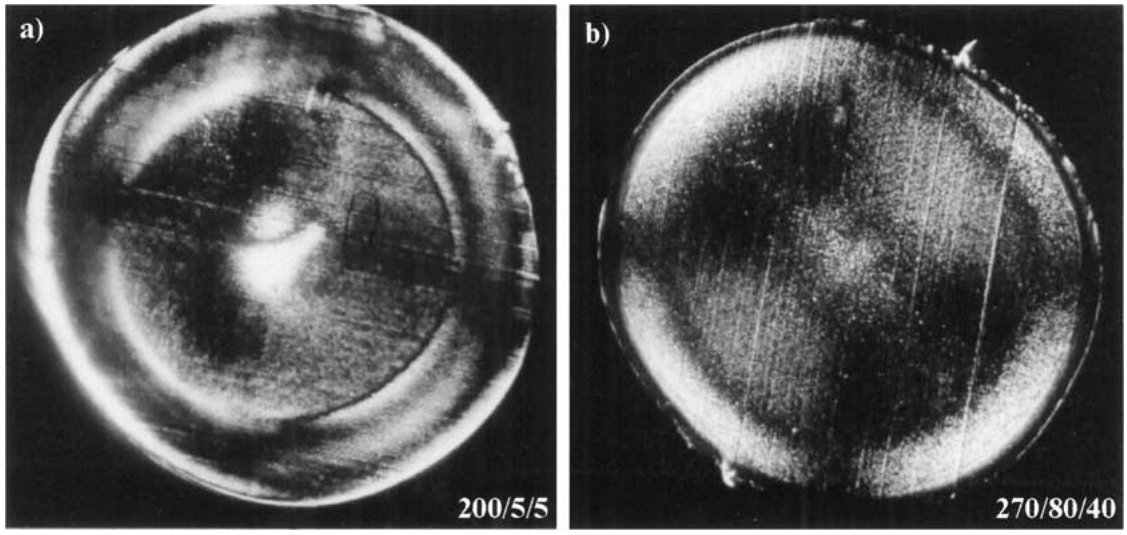

Figure 1 Typical skin-core structures obtained for the extreme moulding conditions: (a) $T_{inj} = 200°C$, $T_m = 5°C$, $Q_{inj} = 5\ cm^3/s$; (b) $T_{inj} = 270°C$, $T_m = 80°C$, $Q_{inj} = 40\ cm^3/s$.

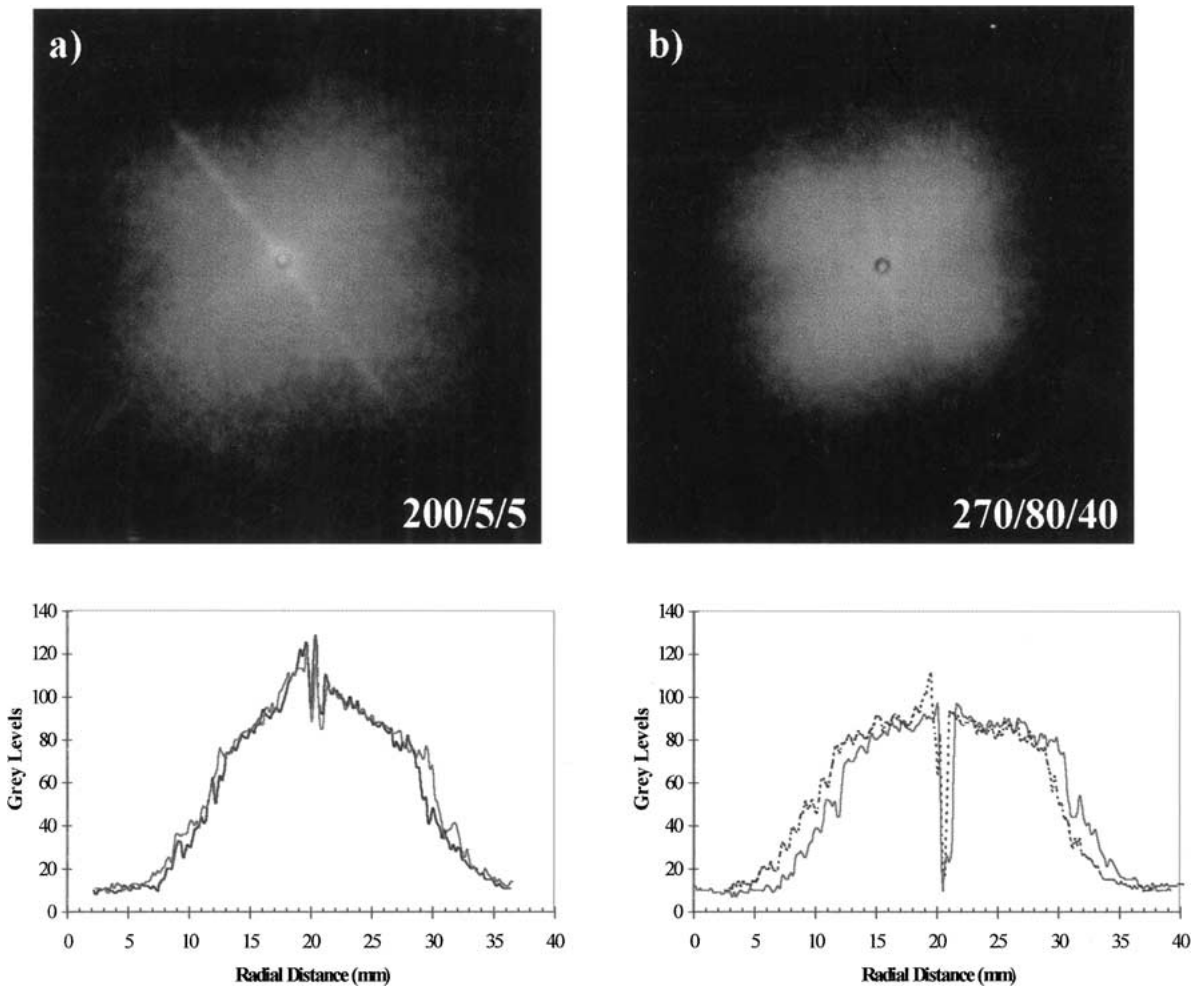

Figure 2 Typical H_v scattered pattern (upper) of the core layer and the respective plot of the grey level variation along the 4 lobes (lower) for the extreme moulding conditions: (a) $T_{inj} = 200°C$, $T_m = 5°C$, $Q_{inj} = 5\ cm^3/s$; (b) $T_{inj} = 270°C$, $T_m = 80°C$, $Q_{inj} = 40\ cm^3/s$.

a better definition of the scattered pattern is shown in the Fig. 2b for the high processing variables setting, which corresponds to an expectable more homogeneous microstructure.

TABLE II Limits of variation and experimental errors on the measurements of the skin ratio, S_a, and the core spherulite sizes, R_s

	Values		Errors (%)	
	S_a	R_s (μm)	S_a	R_s
Average	—	—	7.3	14.1
Maximum	0.643	3.5	11.2	20.9
Minimum	0.114	1.7	4.2	3.2
Variation (%)	463	106	—	—

S_a—skin ratio, R_s—spherulite radius.

The Table II shows the extreme values and the experimental errors on the assessment of S_a and R_s. The selected variations of the processing conditions impart a great change on the two assessed microstructural parameters, mainly on S_a.

4.2. Mechanical characterization

The Table III shows the limits of variation of the mechanical properties at the two test velocities, whereas the experimental errors of the measurements are presented in the Table IV. Comparing the results obtained at both velocities, some differences arise:

a. The mouldings tested at higher velocity show considerably higher values of E and σ_y.

TABLE III Limits of variation of the mechanical properties at the two test velocities of 3.33×10^{-5} (2 mm/min) and 3 m/s

	3.33×10^{-5} m/s (2 mm/min)				3 m/s			
	E (GPa)	σ_y (MPa)	ε_b (mm/mm)	u_b (J/mm^2)	E (GPa)	σ_y (MPa)	ε_b (mm/mm)	u_b (J/mm^2)
Maximum	0.870	38.8	2.29	4.40	4.07	58.8	0.47	0.91
Minimum	0.598	29.0	1.85	3.34	2.40	46.8	0.20	0.33
Variation (%)	46	34	24	32	69	26	132	178

E—initial modulus, σ_y—yield stress, ε_b—strain at break, u_b—energy at break by unit surface area.

TABLE IV Experimental percentual errors on the measurements of the mechanical properties at the two test velocities of 3.33×10^{-5} (2 mm/min) and 3 m/s

	3.33×10^{-5} m/s (2 mm/min)				3 m/s			
(in %)	E	σ_y	ε_b	u_b	E	σ_y	ε_b	u_b
Average	6.1	4.4	1.4	4.6	4.9	3.3	4.3	9.4
Maximum	10.1	1.1	4.0	15.0	10.4	6.0	9.9	16.3
Minimum	3.0	2.7	0.4	1.5	2.1	1.4	1.3	5.0

E—initial modulus, σ_y—yield stress, ε_b—strain at break, u_b—energy at
break per unit of surface area.

TABLE V Coefficients of multiple regression, R^2, and the percentage of residuals of the microstructure-mechanical properties surface fittings (for comparison the average experimental errors, e, are also tabulated)

	2 mm/min				3 m/s			
	E	σ_y	ε_b	u_b	E	σ_y	ε_b	u_b
R^2	0.44	0.62	0.76	0.13	0.20	0.61	0.29	0.15
Residual (%)								
Average	6.1	4.5	2.1	6.7	13.1	3.4	16.9	15.9
Maximum	15.3	14.3	6.4	14.7	25.9	8.0	54.2	79.9
Minimum	0.2	0.3	0.1	0.6	0.7	0.8	4.1	0.6
e (%)	6.1	4.4	1.4	4.6	4.9	3.3	4.3	9.4

E—initial modulus, σ_y—yield stress, ε_b—strain at break, u_b—energy at break by unit surface area.

b. At higher velocity, the deformation and energy absorption capabilities of the mouldings are substantially reduced (much lower values of ε_b and u_b).
c. At higher strain rates, the sensitiveness of the mechanical properties to processing conditions is higher, especially for the case of ε_b and u_b.

5. Discussion

The variations of the mechanical properties with the microstructural parameters (S_a and R_s) will be depictured by response surfaces in the form of 3D graphs. These were obtained by fitting the experimental data to simple polynomial equations, using a least-square minimisation procedure (Tablecurve3D® software). The goodness of the fittings is evaluated by the coefficient of multiple regression, R^2, and by the maximum percentage of the residuals (Table V). The low values of R^2 and the large residuals may suggest that other morphological parameters than S_a and R_s should be considered.

5.1. Initial modulus, E

In the Fig. 3 are shown the variations of the E upon S_a and R_s, for both test velocities, being noticeable the high effect of S_a. The effect of the strain-rate is also clear: E increases significantly for the highest test velocity. As expected, an increase of S_a results in higher values of E, due to a high amount of more oriented material (in the tensile direction). However, the values of the coefficient of multiple regression, R^2, are very small, indicating that other microstructural parameters must also be considered. In fact, it is expected an important contribution of the amorphous phase state for the initial deformation stages.

5.2. Yield stress, σ_y

The Fig. 4 shows the variations of σ_y with S_a and R_s, for both test velocities, evidencing the high dependence on S_a. At higher velocity the values of σ_y are significantly higher. The spherulite size plays again an almost insignificant role. The relative low values of R^2 (nevertheless higher that in the case of the modulus) also indicate that other microstructural parameters should be considered. For compression moulded samples, σ_y has been found to depend on the crystalline phase features, namely on the thickness of the lamellae (and

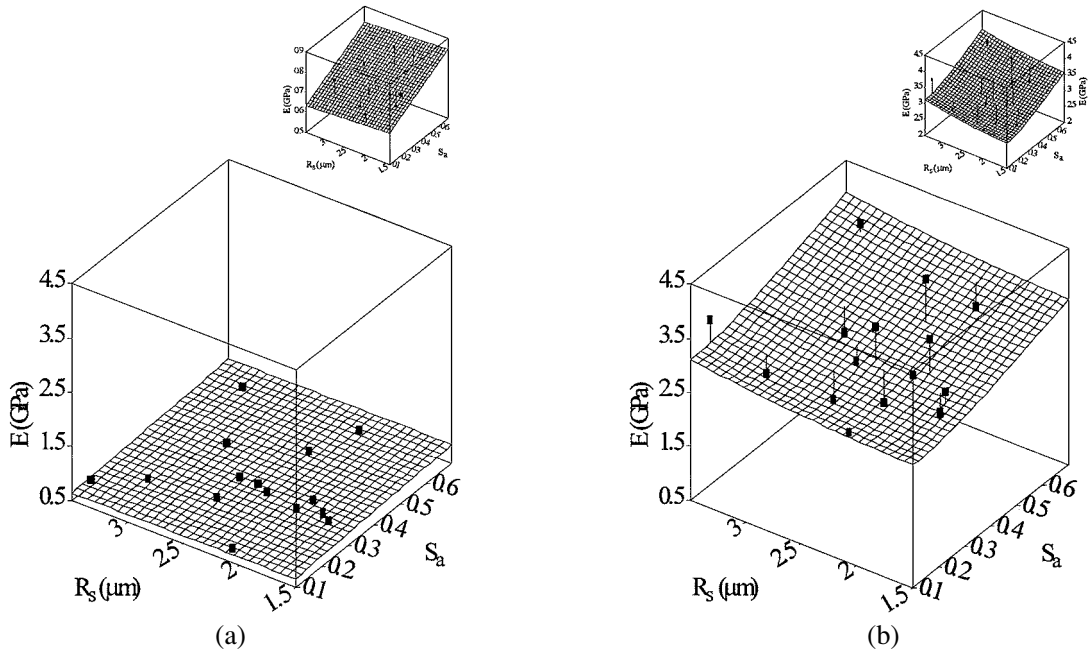

Figure 3 Variation of the initial modulus, E, with the spherulite radius, R_s, and the skin ratio, S_a, for the two test velocities (a) 2 mm/min ($R^2 = 0.44$); (b) 3 m/s ($R^2 = 0.20$) (for clear analysis purposes, the upper graphs are the same results but plotted in different scales).

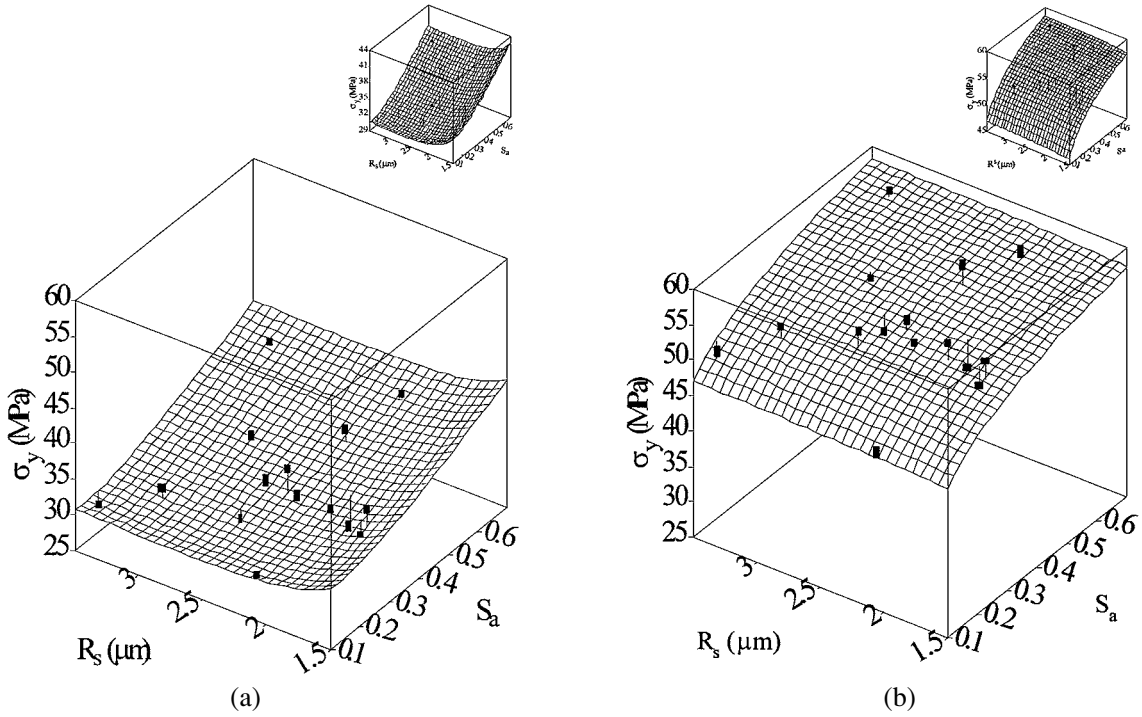

Figure 4 Variation of the yield stress, σ_y, with the spherulite radius, R_s, and the skin ratio, S_a, for the two test velocities (a) 2 mm/min ($R^2 = 0.62$); (b) 3 m/s ($R^2 = 0.61$) (for clear analysis purposes, the upper graphs are the same results but plotted in different scales).

subsequently on the degree of crystallinity) [25]. An increase in S_a results in higher σ_y values due to the increase of more and eventually highly oriented material in the tensile direction.

5.3. Strain at break, ε_b

The variations of the strain at break, ε_b, with S_a and R_s are presented in the Fig. 5, showing also a greater dependence on S_a. The deformation capabilities of the mouldings are notably decreased as the strain-rate increases. For both test velocities, the increase on S_a results in lower ε_b values, due to the lower deformation limits of the already more oriented material. The dependencies of ε_b on R_s are very small, showing however different strain rate sensitivities. At low velocity, ε_b decreases with the increase of R_s, as would be expected [6], whereas it slightly increases for the highest test velocity. This may be an indication of a change on the failure mechanisms with the strain rate. Nevertheless,

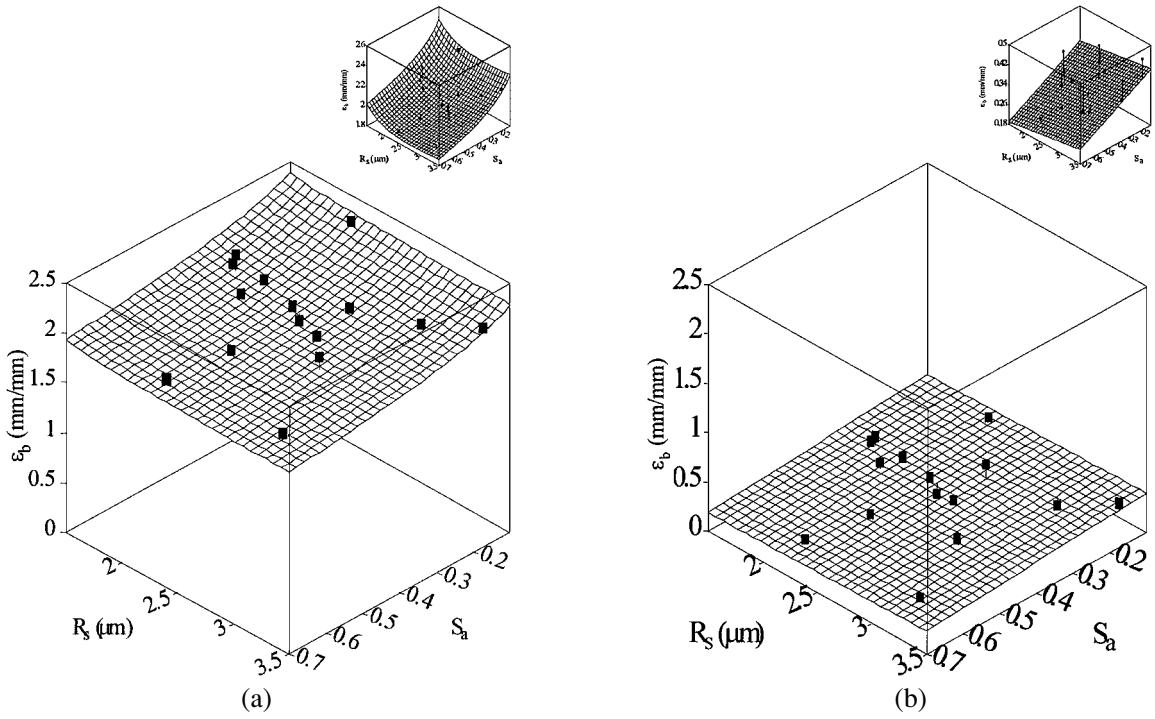

Figure 5 Variations of the strain at break, ε_b, with the spherulite radius, R_s, and the skin ratio, S_a, for the two test velocities (a) 2 mm/min ($R^2 = 0.76$); (b) 3 m/s ($R^2 = 0.29$) (for clear analysis purposes, the upper graphs are the same results but plotted in different scales).

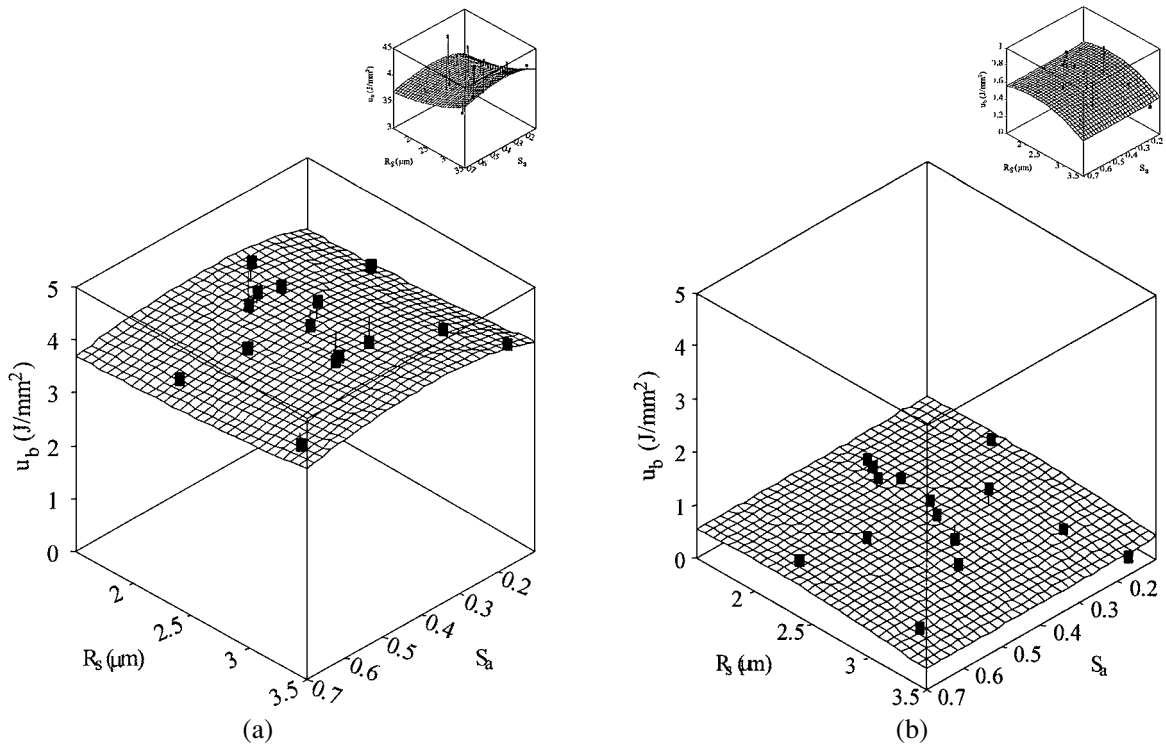

Figure 6 Variation of the energy at break, u_b, with the spherulite radius, R_s, and the skin ratio, S_a, for the two test velocities (a) 2 mm/min ($R^2 = 0.13$); (b) 3 m/s ($R^2 = 0.15$) (for clear analysis purposes, the upper graphs are the same results but plotted in different scales).

and as previously found, the material behaviour cannot be adequably described only with these two microstructural parameters.

5.4. Energy at break, u_b

The Fig. 6 presents the evolution of the energy at break per unit of surface area, u_b, with the two microstructural parameters. As expected, at the lowest velocity the energy absorbed by the mouldings is by far higher than at the impact conditions. The very low values of R^2 suggest a minor contribution of R_s and S_a for the energy absorption capabilities of the mouldings at both strain rates. Nevertheless, the u_b values seem to be more dependent on R_s, in particular at the highest test velocity.

6. Conclusions

For the range of variation of the selected microstructural parameters and for the mechanical properties considered in this work, the following conclusions can be withdrawn:

- At high strain rates, the variations of the mechanical properties are larger, enhancing the microstructural differences.
- The spherulite size of the core is not an important microstructural parameter at both test velocities (at least when these spherulites present small dimensions: 1.5 to 3.5 μm). The mechanical properties are much more dependent on the skin ratio.
- The following microstructure-mechanical properties relationships can be established for both strain rate levels:
  - The modulus increases with S_a.
  - The yield stress increases with S_a.
  - The strain at break decreases with S_a. The dependencies of ε_b on R_s are however dependent on the strain rate.
- Other microstructural parameters of the skin-core laminate microstructure should be taken into account than the selected in this work. For the core region, other feature should be considered, as the spherulite size has a minor contribution. The skin thickness plays an important role, but this parameter should be looked as the amount of oriented material (geometrical feature), and not as a measure of its level of orientation.

Acknowledgments

The authors are grateful to the Programme of Scientific and Technical cooperation between ICCTI and the French Embassy in Portugal.

References

1. M. R. KANTZ, H. D. NEWMAN and F. H. STIGALE, *J. Apply. Polym. Sci.* **16** (1972) 1249.
2. S. S. KATTI and J. M. SCHULTZ, *Poly. Eng. Sci.* **22**(16) (1982) 1001.
3. M. FUJIYAMA, in "Polypropylene Structure, Blends and Composites: Structure and Morphology," edited by J. Karger-Kocsis, (Chapman & Hall, London, 1995) Vol. 1, chap. 6, p. 167.
4. A. M. CUNHA and A. S. POUZADA, in "Impact and Dynamic Fracture of Polymers and Composites," edited by J. G. Williams and A. Pavan, ESIS19, (Mechanical Eng. Public, 1995) London, p. 315.
5. J. C. VIANA, A. M. CUNHA and N. BILLON, *Poly. Eng. Sci.* **39** (1999) 1463.

6. J. L. WAY, J. R. ATKINSON and J. NUTTING, *J. Mater. Sci.* **9** (1974) 293.
7. K. FRIEDERICH, *Kunststoffe* **69**(11) (1979) 796 (English trans. pp. 17–19).
8. R. PHILLIPS, G. HERBERT, J. NEWS and M. WOLKOWICZ, *Polym. Eng. Sci.* **34**(23) (1994) 1731.
9. M. FUJIYAMA and T. WAKINO, *Intern. Polym. Proc.* **VII**(2) (1992) 159.
10. M. OUEDERNI and P. J. PHILLIPS, SPE ANTEC Tech. Papers, ANTEC'96, 1996.
11. A. M. CUNHA, A. S. POUZADA and R. J. CRAWFORD, *Plast. Rub. Comp. Proc. Appl.* **18** (1992) 79.
12. J. S. ZAROULIS and M. C. BOYCE, *Polymer* **38**(6) (1997) 1303.
13. J. C. VIANA, A. M. CUNHA and N. BILLON, *Poly. Int.* **43** (1997) 159.
14. *Idem.*, N., in Proceedings 10th Int. Conf. Deformation, Yield and Fracture of Polymers, Cambridge, U.K., 1997, p. 320.
15. G. KALAY, and M. J. BEVIS, *J. Polym Sci.: Part B: Polym. Phys.* **35** (1997) 265.
16. W. WENING and F. HERZOG, *J. Appl. Polym. Sci.* **50** (1993) 2163.
17. J. C. VIANA, Ph.D. Thesis, University of Minho, 2000.
18. M. FUJIYAMA and T. WAKINO, *Intern. Polym., Proc.* **VII**(1) (1992) 97.
19. J.-P. TROTIGNON and J. VERDU, *J. Appl. Polym. Sci.* **34** (1987) 1.
20. P. ZIPPER, P. M. ABUJA, A. JÁNOSI, E. WRENTSCHUR, W. GEYMAYER, E. INGOLIC and W. FRIESENBICHLER, *Polym. Eng. Sci.* **36**(4) (1996) 467.
21. S. C. TJONG, J. S. SHEN and R. K. Y. LI, *ibid.* **36**(1) (1996) 100.
22. J. VARGA, I. MUDRA and G. W. EHRENSTEIN, SPE ANTEC Tech. Papers, ANTEC'98, 1998, p. 3492.
23. Y. P. KHANAN, *Macromolecules*, **26** (1993) 3639.
24. J. M. HAUDIN, in "Optical Properties of Polymers," edited by G. H. Meeten (Elsevier Science Publishers, London, 1989) chap. 4 p. 167.
25. N. W. BROOKS, M. GHAZALI, R. A. DUCKETT and A. P. UNWIN, *Polymer* **40** (1999) 821.

Received 3 August 2000
and accepted 24 April 2001